TISSUE ENGINEERING: Part C
Volume 19, Number 12, 2013

DOI: 10.1089/ten.tec.2012.0741

Optimum Parameters for Freeze-Drying Decellularized Arterial Scaffolds

William S. Sheridan, BEng,[1,2] Garry P. Duffy, PhD,[1,3] and Bruce P. Murphy, PhD[1,2]

Decellularized arterial scaffolds have achieved success in advancing toward clinical use as vascular grafts. However, concerns remain regarding long-term preservation and sterilization of these scaffolds. Freeze drying offers a means of overcoming these concerns. In this study, we investigated the effects of various freeze-drying protocols on decellularized porcine carotid arteries and consequently, determined the optimum parameters to fabricate a stable, preserved scaffold with unaltered mechanical properties. Freeze drying by constant slow cooling to two final temperatures ((T_f), $-10°C$ and $-40°C$) versus instant freezing was investigated by histological examination and mechanical testing. Slow cooling to $T_f = -10°C$ produced a stiffer and less distensible response than the non freeze-dried scaffolds and resulted in disruption to the collagen fibers. The mechanical response of $T_f = -40°C$ scaffolds demonstrated disruption to the elastin network, which was confirmed with histology. Snap freezing scaffolds in liquid nitrogen and freeze drying to $T_f = -40°C$ with a precooled shelf at $-60°C$ produced scaffolds with unaltered mechanical properties and a histology resembling non-freeze-dried scaffolds. The results of this study demonstrate the importance of optimizing the nucleation and ice crystal growth/size to ensure homogenous drying, preventing extracellular matrix disruption and subsequent inferior mechanical properties. This new manufacturing protocol creates the means for the preservation and sterilization of decellularized arterial scaffolds while simultaneously maintaining the mechanical properties of the tissue.

Introduction

The science of tissue-engineered vascular grafts has developed significantly since the creation of the first construct by Weinberg and Bell.[1] However, producing a vessel substitute that is safe and clinically successful in a timely and cost-effective regulatory controlled manufacturing environment still remains a challenge. Currently, the internal mammary artery or saphenous vein remains the autologous substitute vessels of choice for bypass grafting, once catheter-based treatment modalities have been exhausted.[2,3] Host vessel availability is limited in a large number of patients, implying that there is an obvious need for a durable alternative.

Recently, the use of exogenous decellularized tissue has shown promising clinical applicability.[4–6] Decellularized vascular tissue has demonstrated great potential due to its mechanical properties, nonimmunogenicity, and ability to remodel and grow[7–9]; moreover, vascular scaffolds have already demonstrated feasibility *in vivo* with good patency rates.[10,11] Issues associated with translating these scaffolds to a clinical environment will be as follows: reducing the manufacturing times, producing a range of geometries to accommodate a large patient cohort, creating methods for long-term preservation (to produce a reasonable shelf life), and appropriate sterilization techniques. Lyophilization (freeze drying) offers a potential solution to these issues, as it produces a completely dry, stable scaffold that can be easily sterilized with ethylene oxide or gamma radiation.[10,12,13]

Controlling the crystal nucleation rate and crystal size is essential when freeze drying biological tissue, as excessive crystal growth and size can disrupt extracellular matrix (ECM) components and create tissue heterogeneity.[14,15] The importance of determining the ideal freeze-drying parameters to preserve the ECM has been demonstrated for other biological tissues such as decellularized heart valves[12] and bovine pericardium.[16] Some studies have investigated the use of additional agents to preserve structure during both freezing and freeze drying.[12,17,18] However, cryoprotective agents have largely been used to preserve cell function, which is not relevant with the use of decellularized tissue. Lyoprotectants have been shown to stabilize proteins and liposomes during freeze drying,[18] but their use with whole tissue structure has not been widely studied. Therefore, in this study, we strived to determine an optimum protocol by altering freeze-drying parameters alone, without the use of cryoprotective agents and/or lyoprotectants.

[1]Trinity Centre for Bioengineering, Trinity Biomedical Sciences Institute, Trinity College Dublin, Dublin, Ireland.
[2]Department of Mechanical and Manufacturing Engineering, School of Engineering, Trinity College Dublin, Dublin, Ireland.
[3]Department of Anatomy, Royal College of Surgeons in Ireland, Dublin, Ireland.

This study focuses on determining the effects of the freeze-drying process on the mechanical integrity of decellularized porcine carotid arteries. We hypothesized that altering the freeze-drying parameters, namely freezing rate and final temperature, will disrupt the ECM, resulting in altered scaffold mechanical properties. Constructs manufactured by constant slow cooling to two final temperatures or instant snap freezing in liquid nitrogen with final freeze-drying temperature of $T_f = -40°C$ were investigated by a histological examination and biomechanical testing.

Methods and Materials

Tissue harvest

Carotid arteries were freshly harvested from 70 to 90 kg pigs in a local abattoir (Lislin Meats Ltd, Mullagh, Co.). Common carotid arteries 5–7 mm in diameter were extracted from each pig. All arteries were returned to the laboratory and stored in phosphate-buffered saline (PBS) on ice. Samples were prepared by removing excess connective and adventitial tissue and cut into approximately 30 mm-long segments. Next, all samples were frozen in PBS at −20°C for later use, as it had been previously shown that freezing does not affect the mechanical properties of porcine tissue.[19]

Decellularization

Decellularization was carried out as previously described.[20] The scaffolds produced using this protocol are referred to here as standard decellularized scaffolds. This standard protocol was used, as it produces an unaltered ECM, with similarities to most decellularization protocols, and has been used by a number of research groups.[8,21,22] Briefly, samples were immersed in de-ionized water for 24 h at 4°C under rotational agitation and, subsequently, incubated in 0.05% Trypsin with 0.02% EDTA (Sigma-Aldrich) for 1 h at 37°C. Next, the samples were placed in a solution of 2% Triton X-100 and 0.8% ammonium hydroxide (Sigma-Aldrich) in de-ionized water for 72 h at 4°C with a daily solution change and a final wash sequence of 48 h in de-ionized water, all of which were under rotational agitation.

A second group of scaffolds were prepared as previously described[20]; this was a manipulated scaffold to increase cell infiltration, and these scaffolds are referred to here as customized scaffolds. The protocol was exactly as described earlier but with the additional step of selectively decreasing collagen content by sodium hydroxide (NaOH) digestion. This additional step occurred after the 72 h of agitation in the decellularization solution. The samples were immersed in 0.5 M NaOH and sonicated for 90 min at room temperature. The final wash sequence of 48 h took place after this. All samples from both groups were frozen in PBS at −20°C immediately after decellularization.

Freeze-drying cycles

Three different freeze-drying cycles were investigated (see Fig. 1A):

1. $T_f = -10°C$

A constant cooling rate during freezing of 1°C/min to a final temperature of −10°C, followed by a 60 min hold at this temperature. A 4 h ramp to 0°C under vacuum of 200 mTorr and 17 h at 0°C and secondary drying at 20°C at the same pressure.

2. $T_f = -40°C$

The same protocol as $T_f = -10°C$ earlier, except a final temperature of −40°C, was reached.

3. $SF\ T_f = -40°C$

The same protocol as $T_f = -40°C$, except the freeze-dryer shelf, was precooled to −60°C before commencement of the cycle.

Before freeze drying, all samples were thawed rapidly in a water bath at 37°C and then incubated at room temperature for >1 h in the PBS in which they had been originally frozen. Each sample, for cycles $T_f = -10°C$ and $T_f = -40°C$, was positioned on a stainless steel mandrel (Fig. 1B), suspended on a stainless steel tray, and placed on the shelves of the freeze dryer (Virtis Genesis 25EL; Biopharma). Samples for SF $T_f = -40°C$ were removed from PBS, air dried for 1 min to remove excess fluid, placed in tubes, and snap frozen in liquid nitrogen. Before placement within the freeze drier, the mandrels, tray, and tweezers used to mount the samples were cooled to −60°C for 1 h. Each freeze-drying cycle was applied to both the decellularized and customized scaffolds.

Histology

5 mm ring segments were taken from each group for histological analysis. Samples were embedded in paraffin wax in an automatic tissue processor (ASP300; Leica). Samples were sectioned longitudinally using a rotary microtome (Leica microtome; Leica). 7 μm sections were cut and collected on glass slides and, subsequently, washed through a graded series of ethanol from 100 to 70% (v/v). Native and decellularized tissue was stained using Hematoxylin and Eosin (H&E) and Veorhoff Van Geison. Sections were dehydrated and cleaned in ascending concentrations of ethanol and xylene before coverslips were mounted (DPX mountant, BDH). Observation under light microscopy and digital image acquisition was carried out with an inverted microscope (Olympus IX 71).

Mechanical testing

Tensile tests. Uniaxial tensile tests were carried out on scaffolds that were subjected to each of the freeze-drying cycles for both decellularized and customized scaffolds as previously described.[20] Non-freeze-dried native tissue, decellularized scaffolds, and customized scaffolds were also tested as controls. The tests were performed using a Zwick tensile testing machine (Zwick Z005; Roell). Freeze-dried samples were re-hydrated in PBS for >1 h, and intact ring sections that were 4 mm long were cut from each sample ($n = 10$), mounted on custom-made grips, and tensile tested to failure at a rate of 2 mm/min using a 100 N load cell. All samples were preconditioned to a force of 0.1 N before commencement of the test. Video extensometer tracking was used to determine the true stress and true strain as previously described.[17] 3rd-order polynomial regression curves were applied to the raw data and averaged to determine the overall mechanical response. A linear elastic response was observed in the first and final third of the stress–strain data, corresponding to the elastin dominant phase and collagen

dominant phase, respectively. The slope of the fitted linear responses to the first third and last third of the stress strain data defined the moduli for each phase.

Opening angle measurement. Opening angle measurements were undertaken to determine the effects of freeze drying on the residual strain within the scaffold wall.[23] Ring sections that were 2–3 mm in length were cut from re-hydrated freeze-dried samples. Each sample was placed in a well of a 24-well plate and submerged in PBS at room temperature. After 30 min, the sample was removed, placed on a chopping board, and cut open by a single radial cut. The sample was returned to the well plate to equilibrate for 30 min, after which an image was recorded. The opening angle was defined as the angle (θ) formed from the midpoint of the inner circumference to the end points of the inner circumference (Fig. 6B). ImageJ software (US National Institutes of Health) was used to determine this angle from the raw image. In the case of large recoil in the sample, θ was measured in the same manner but was given a negative value (Fig. 6D), $n = 10$ for all groups.

Suture retention strength. Suture retention strength was determined at room temperature. Freeze-dried samples were re-hydrated in PBS for >1 h before testing ($n = 6$). The sample was secured at the bottom of the test machine using a custom-built grip that allows uniform clamping. A single suture (3–0 Tevdek® II, Teleflex Medical) was inserted 5 mm from the scaffold edge, passed through a hook in the top grip, and securely fastened. The suture was pulled from the tissue at a rate of 10 mm/min until rupture, and the maximum force reached was recorded as the suture retention strength.

Statistics

Box plots were used to present the distributions of the data. Each box displays interquartile range (IQR) with median, and outliers (defined as median ± 1.5*IQR) are shown with individual dots. A student's *t*-test was used to test significance between each group separately, and results with $p < 0.05$ were considered statistically significant.

Results

Freeze drying

Freeze drying in all scaffold groups produced a uniformly dried, brittle scaffold that conformed well to the stainless steel mandrel (Fig. 1B). Scaffolds slid off the mandrel with minimal force to reveal an intact, dried scaffold with a reduced wall thickness due to removal of solute (Fig. 1C). Figure 2 shows the results of H&E staining for all groups. The $T_f = -10°C$ group displayed inconsistent and uneven drying across the scaffold wall (Fig. 2D). The porous nature of the scaffold in the wall center contained separated collagen fiber bundles, which are not apparent at the scaffold edges where collagen fiber bundles are compressed together. There was also evidence of disruption of the collagen fiber network within the center of the scaffold wall. Figure 3 details the disruption to the ECM after freeze drying with native and decellularized tissue displayed for comparison. The intact undulating nature of the collagen fibers was apparent in the native tissue and maintained after decellularization (Fig. 3A, B). Rupture of a large number of collagen fiber bundles was clear and highlighted in Figure 3C (black arrows). The customized scaffold also showed evidence of fiber disruption (Fig. 2G), but this damage is less severe than the decellularized scaffold (Fig. 3D). The drying process appears consistent for the customized scaffolds and evenly distributed across the scaffold wall. $T_f = -40°C$ displayed markedly less fiber disruption than $T_f = -10°C$. For decellularized scaffolds (Fig. 2E), the collagen fiber bundles were clearly intact; however, inconsistent drying appears across the scaffold wall, particularly on the luminal side where loosening of the ECM is evident. Veorhoff Van Geison staining further revealed disruption to the elastin network, which was not immediately obvious from the H&E staining. Elastin fibers were stained black by this stain, and fragmentation of the elastin sheets was clear within the decellularized scaffolds that were subjected to $T_f = -40°C$ (Fig. 3F). Minor collagen fiber damage was seen in the customized scaffolds with the same freeze-drying cycle (Fig. 2H), while homogenous drying was seen across the scaffold wall. All scaffolds that had been subjected to SF $T_f = -40°C$ produced a homogenous structure with minimal ECM disruption (Fig. 2F, I). Minimal fiber disruption was observed

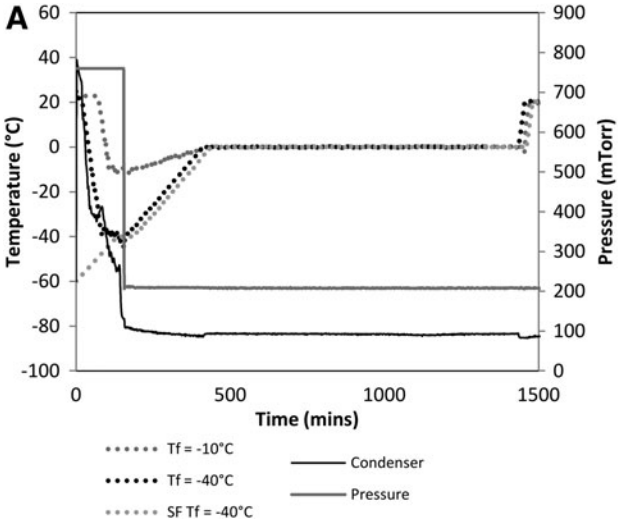

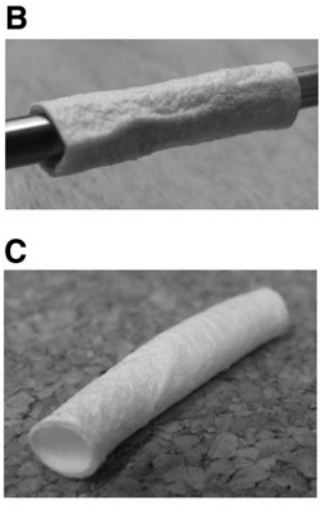

FIG. 1. Freeze drying of decellularized vascular scaffolds. **(A)** Three freeze-drying protocols were investigated, $T_f = -10°C$, $T_f = -40°C$ and snap frozen samples in a precooled −60°C chamber to $T_f = -40°C$. **(B)** Freeze-dried sample on mandrel ensures even drying. **(C)** Scaffold retains shape after removal from mandrel.

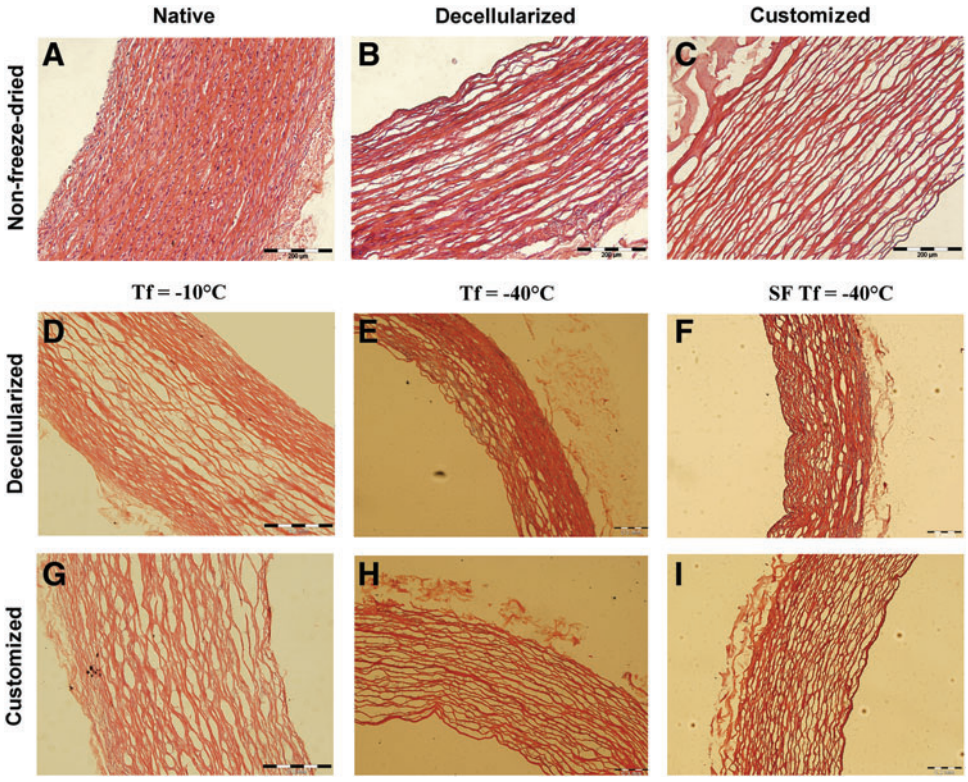

FIG. 2. Effects of freeze drying on decellularized and customized scaffolds. **(A)** Highly cellular non-freeze-dried native tissue. **(B)** Cell removal reveals a porous intact ECM after decellularization. **(C)** Decreased matrix density is evident after customization. **(D)** Decellularized scaffolds in the $T_f = -10°C$ group display a nonhomogenous matrix with fiber rupture within the wall center. **(E)** $T_f = -40°C$ shows markedly less fiber disruption than $T_f = -10°C$. **(F)** SF $T_f = -40°C$ produced a homogenous structure with minimal ECM disruption for the decellularized scaffolds. **(G)** The $T_f = -10°C$ customized scaffold showed evidence of fiber disruption but not as severe as the decellularized scaffold. **(H)** Fiber damage was visible for the customized scaffolds in the $T_f = -40°C$ group with consistent drying. **(I)** SF $T_f = -40°C$ customized scaffolds resembled the non-freeze-dried scaffolds with homogenous drying. All scale bars indicate 200 μm. Color images available online at www.liebertpub.com/tec

under high magnification (Fig. 3E), where the ECM after freeze drying appears comparable to non-freeze-dried scaffolds.

Mechanical test results

Tensile tests. The stress–strain curves of all of the scaffolds tested displayed a hyperelastic response that was typical of a biological soft tissue.[24,25] The standard scaffold $T_f = -10°C$ group produced a much reduced elastin region and a short transition, leading to a stiffer collagen region (Fig. 4A). $T_f = -40°C$ displayed a different response with a much extended elastin region, shifting the transition region to much higher strain values and ending with a normal collagen phase. Moreover, a significant reduction in the modulus of the elastin phase and a similar collagen-phase modulus was observed in this group in comparison to the standard decellularized group (Fig. 5A). There is no significant difference between the collagen-phase modulus and the non-freeze-dried scaffolds for SF $T_f = -40°C$ except for the customized scaffolds (Fig. 5A). However, there was a significant reduction for the $T_f = -40°C$ versus the standard decellularized group (Fig. 5B).

The customized scaffolds exhibit some alterations in the mechanical response after freeze drying (Fig. 4B). $T_f = -10°C$ produced a less distensible response with a reduced toe region and an early transition region. Similarly, for $T_f = -40°C$, an earlier transition region was observed, which was stiffer than the non-freeze-dried scaffolds. The SF $T_f = -40°C$ scaffolds matched closely the response of the non-freeze-dried scaffolds with a comparable elastin and transition region, while the collagen phase was noticeably stiffer on the curve and the collagen-phase modulus was significantly different (Fig. 5B). The elastin-phase moduli for both the decellularized and customized scaffolds were not significantly altered after freeze drying.

Opening angle measurement. Native tissue displayed the largest opening angle on release of the residual stress; however, the customized scaffolds had a significantly lower opening angle than the decellularized scaffolds and native tissue specimens with recoil extending below the original diameter (see Fig. 6). Decellularized scaffolds displayed a reduction in residual stress for each of the freeze-drying cycles with no statistical significant difference for any cycle. Customiszd scaffolds had a statistically significant decrease in opening angle for each freeze-drying cycle in comparison to native tissue.

Suture retention strength. The maximum force to pull a suture through a scaffold wall to failure for each of the groups tested is shown in Figure 7. The maximum average

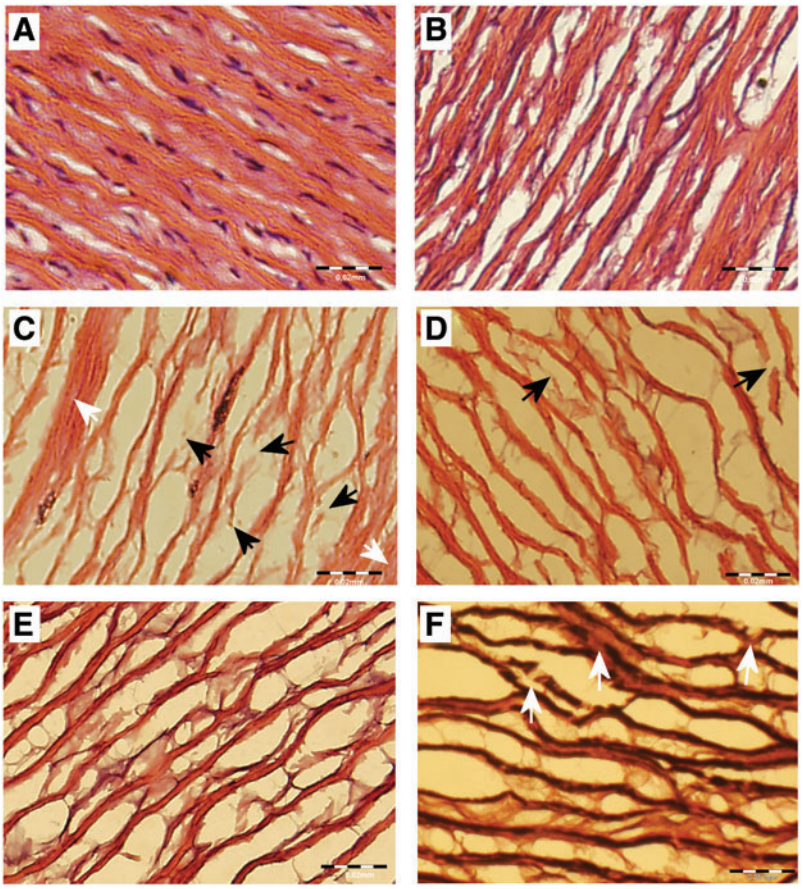

FIG. 3. ECM disruption as a result of freeze drying. **(A)** H&E staining of native tissue reveals highly dense undisrupted nature of collagen fibers. **(B)** Decellularization does not disrupt fibers **(C)** H&E staining shows that $T_f = -10°C$ causes major collagen fiber disruption in decellularized scaffolds; black arrows indicate fully ruptured fibers; and white arrows display areas of nonuniform drying. **(D)** Less fiber damage was visible in $T_f = -40°C$ decellularized scaffolds, but more uniform drying was apparent. **(E)** SF $T_f = -40°C$ customized scaffolds retained a similar configuration of ECM as non-freeze-dried scaffolds. **(F)** Verhoff Van Gieson staining of decellularized scaffold in the $T_f = -40°C$ group displayed disruption of the elastin network (elastin fibers stain black). Fragmentation of the elastin sheets was visible (white arrows). Scale bars in **A–C** indicate 20 μm and 50 μm in **D**. Color images available online at www.liebertpub.com/tec

forces for native tissue, decellularized and customized decellularized scaffolds were $1.8\,N \pm 0.41$, $1.8\,N \pm 0.42$, and $1.9\,N \pm 0.49$, respectively. The suture retention strength was similar across all freeze-drying cycles to these controls, except $T_f = -40°C$ for decellularized scaffolds. There was a significant difference compared with the native and decellularized controls for $T_f = -40°C$.

Discussion

Currently, there are a number of vascular tissue-engineering techniques obtaining impressive *in vivo* results, and they have the potential to advance toward routine clinical use.[26,27] While these techniques can vary in their individual approaches, they are principally overcoming difficulties such as obtaining suitable architecture with appropriate mechanical properties and cell adhesion characteristics and are nonimmunogenic and nonthrombongenic.[28] However, regardless of the technique utilized, there are certain additional criteria that any tissue-engineered constructs should meet, namely quick and efficient manufacturing, availability in various diameters and lengths, long-term preservation for simple storage and transport, adequate sterilization techniques, and overall ease of use.

We have previously provided a means of bulk cell seeding the medial layer of customized decellularized scaffolds that has the potential to greatly reduce manufacturing times[20]; however, we did not address the issues of sterilization and long-term preservation. To incorporate shelf-life concerns and sterilization protocols, we have investigated a number of freeze-drying techniques. It has previously been shown that ethylene oxide[10,29] and gamma radiation[13,30,31] are suitable methods for sterilizing freeze-dried biological tissue for eventual use *in vivo*. However, no freeze-drying protocols have been investigated to determine the optimum parameters that will maintain the micro-architecture and mechanical properties of the decellularized vascular scaffold.

Decellularized vascular tissue comprises a compacted highly dense structure. The sublimation of ice crystals from within the layered structure and orientation of the collagen and elastin networks will not merit the formation of pores in the traditional sense in homogenous solutions, but may manifest as damage to the ECM components due to their intricate, interlinked orientations. The use of lyoprotectants during freeze drying have previously been observed to preserve physical characteristics of proteins and liposomes.[32,33] Wang *et al.* have recently shown that sucrose is beneficial in preserving the mechanical response of decellularized heart valves[12]; however, some alteration to the pore size and ECM structure were evident. Very few studies in the literature utilize lyoprotectants in whole tissue structures. Moreover, the importance of determining the appropriate freeze-drying parameters for the preservation of a biological structure has been previously demonstrated.[16] We did not investigate the use of lyoprotectants and focused on determining the optimum freeze-drying parameters alone to ensure a preserved scaffold structure with appropriate mechanical properties.

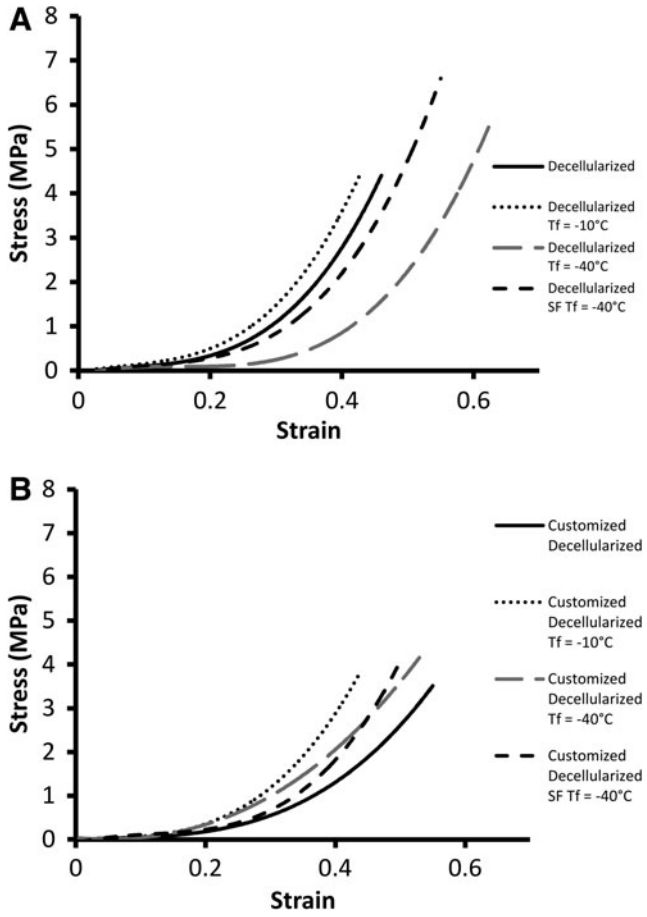

FIG. 4. Stress–strain curves of freeze-dried scaffolds showing the mechanical response of the scaffolds **(A)** Decellularized scaffolds for $T_f = -10°C$ produced a stiffer and less distensible response with an earlier than normal transition to the collagen region. $T_f = -40°C$ displays a markedly different response with a large shift in the transition region of the graph extending the elastin dominant phase. SF $T_f = -40°C$ matches closely the response of the non-freeze-dried scaffolds, particularly in the elastin dominant phase. **(B)** Customized scaffolds for $T_f = -10°C$ produced a stiffer response with a much earlier transition region; similarly, for $T_f = -40°C$, an earlier transition region was seen with a less stiff collagen region. SF $T_f = -40°C$ matched the response of the non-freeze-dried scaffolds for the elastin region, but an altered stiffer response was evident in the collagen phase.

$T_f = -10°C$ was the least effective freeze-drying cycle producing a nonhomogenous structure for both the decellularized and customized scaffolds. The evidence of uneven drying in the decellularized scaffolds was apparent in the histology where ice crystal growth was clearly larger at the center of the scaffold wall, which led to collagen fiber disruption (Fig. 2D). Although more homogenous drying was evident for customized scaffolds, fiber damage was still visible (Fig. 2G). The consequence of this uneven drying was also seen in the mechanical response of the tissue. $T_f = -10°C$ scaffolds were stiffer and less distensible with earlier engagement of collagen fibers seen at the shortened toe region and early transition region on the stress–strain curve (Fig. 4A,B). The mechanical response of the freeze-dried customized scaffolds more closely matches the response of their non freeze-dried controls; this is in comparison to the decellularized scaffolds that see increased deviations from their non-freeze-dried controls. The slightly improved result seen in the customized scaffolds may indicate that the increased solute within the tissue due to the decreased density allows more homogenous nucleation and ice crystal growth.

Overall, in the $T_f = -40°C$ group, less damage was visible with H&E staining. However, uneven drying was evident in the decellularized scaffolds. On further investigation, the tensile tests reveal that there was a large change in the mechanical response of these scaffolds. The greatly extended toe region of the graph signifies elastin damage (Fig. 4A), which was confirmed with the Verhoff Van Geison staining for elastin (Fig. 3F) and a significant difference between the elastin region modulus and the non-freeze-dried control. The customized scaffolds produced an altered shift in the mechanical response, with an earlier than normal transition to the collagen phase; however, this altered response was much less severe than the decellularized scaffold. Fiber damage was visible from the histology but less drastic than the customized scaffolds from the $T_f = -10°C$ group. The excessive disruption for the decellularized group may be a result of the higher density of the matrix. The tightly packed matrix has less solute space and will result in nonuniform nucleation throughout the wall, causing less contiguous, more numerous, and less evenly distributed crystal growth. The nonuniform nucleation and growth of these smaller ice crystals will reduce sublimation and heat-transfer efficiency, which results in the visible uneven drying as seen in the scaffold heterogeneity. It is postulated that the less dense nature of the customized scaffold will negate this nonuniform nucleation, resulting in contiguous more evenly distributed ice crystals. For this reason, scaffold heterogeneity is not seen in the histology (Fig. 2H), and the mechanical response of the customized scaffold does not display excessive elastin network disruption.

The SF $T_f = -40°C$ cycle initiated instant uniform nucleation and small crystal growth throughout the scaffolds. The freeze-drier shelf was precooled to $-60°C$ to ensure the scaffolds remain at the lowest temperature possible ($\leq -60°C$). The SF $T_f = -40°C$ cycle produced overall optimum results. Minimal fiber damage was evident from the histology for both the decellularized and customized scaffolds (Fig. 2F,I), and the mechanical response of both scaffolds most closely matched that of their controls (Fig. 4A,B). In particular, both the elastin phase and transition region are comparable to the controls, indicating an undisrupted elastin network, and there was no significant difference in the modulus for the elastin phase for each of the scaffolds. The process of snap freezing the scaffolds in liquid nitrogen creates extremely small ice crystals, which should create the same issues of nonuniform nucleation and crystal growth, heterogeneity, and ECM damage in the highly dense decellularized scaffolds as in $T_f = -40°C$. However, the additional step of precooling the freeze-drier shelf negates this. Ideal sublimation occurs when ice crystals are large, wide, and contiguous, and this is less likely to occur in a dense matrix structure that is rapidly frozen. Small ice crystals are less thermodynamically stable due to the reduction in surface area/volume. However, since the precooled shelf was at $-60°C$ and the first step of the freeze-drying cycle allows

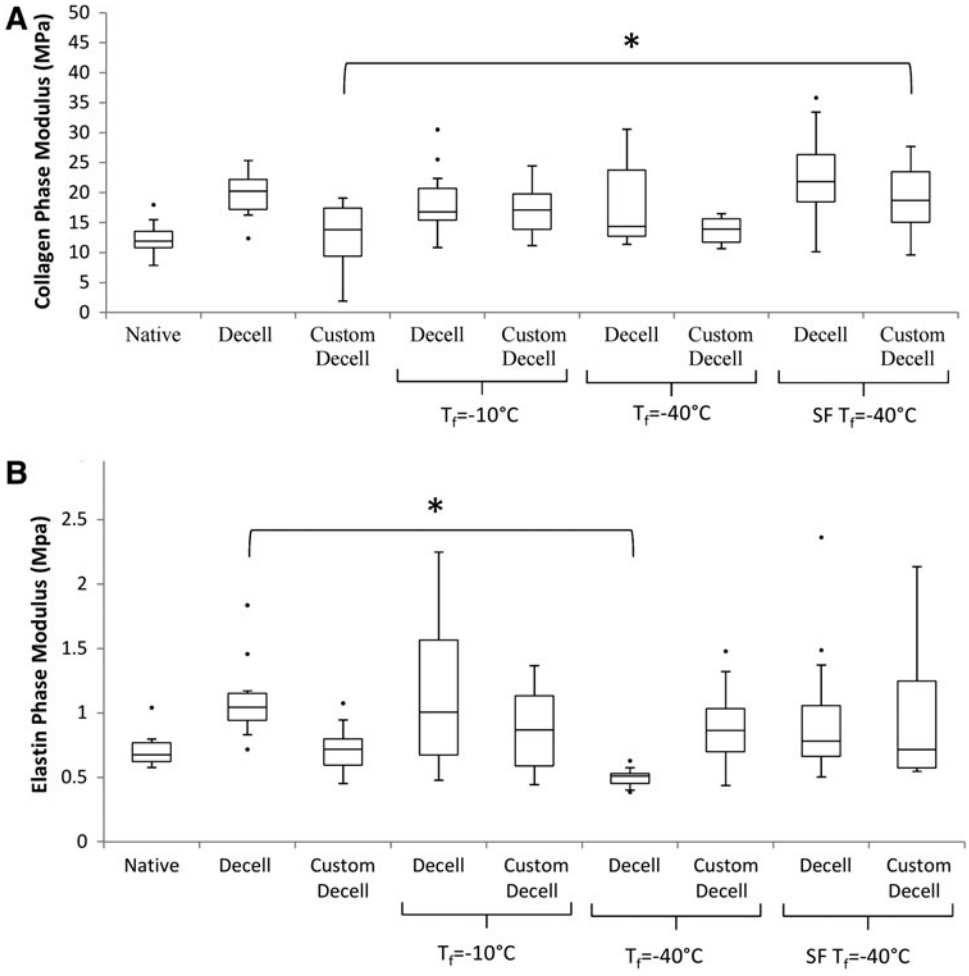

FIG. 5. Collagen and elastin-phase moduli of native, decellularized, customized, and freeze-dried scaffolds. **(A)** Decellularization does not alter the collagen-phase modulus, while customization does. Freeze drying did not significantly affect the collagen modulus in any of the freeze-dried groups except the customized SF $T_f = -40°C$. **(B)** Decellularization increases the elastin-phase modulus, while customization reverses it toward the native modulus. $T_f = -40°C$ significantly reduces the elastin-phase modulus for decellularized tissue, below both the native and decellularized moduli. However, SF $T_f = -40°C$ maintains the elastin modulus for both decellularized and customized decellularized scaffolds. Statistical significance is indicated as $*p < 0.05$.

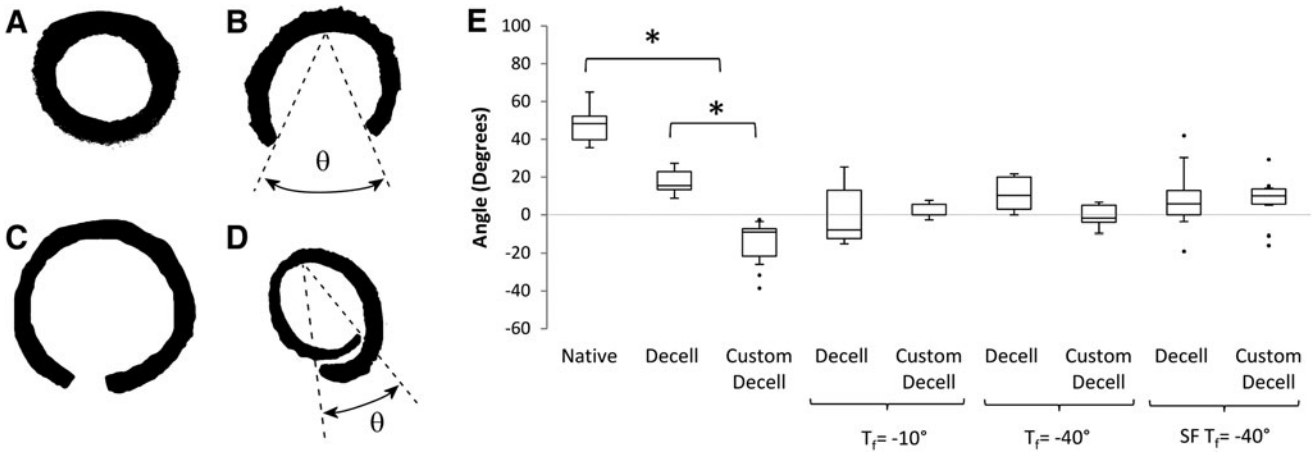

FIG. 6. Opening angle measurement to determine residual stress within scaffolds. **(A)** Intact scaffold in stressed state. **(B)** Native scaffold in zero stress state achieved by radial cut of ring section producing an opening angle θ. **(C)** Decellularized scaffolds displayed a reduced value for θ compared with native scaffolds. **(D)** Customized scaffolds revealed an excessive reduction in θ to the extent that the scaffold recoiled beyond the diameter of the zero stress state. These θ values are taken as negative. **(E)** Boxplot of opening angles for each freeze-drying cycle. Decellularized scaffolds display a significant reduction in θ compared with the native tissue. Customized scaffolds see a significant decrease in θ due to collagen digestion, compared with both native tissue and decellularized scaffolds. Freeze drying reduces the opening angle for the decellularized scaffolds and increases this angle for each of the customized scaffolds, which can be attributed to collagen fiber damage and scaffold heterogeneity. The opening angles of the SF $T_f = -40°C$ scaffolds are reverted back toward that of the native tissue. Statistical significance is indicated as $*p < 0.05$.

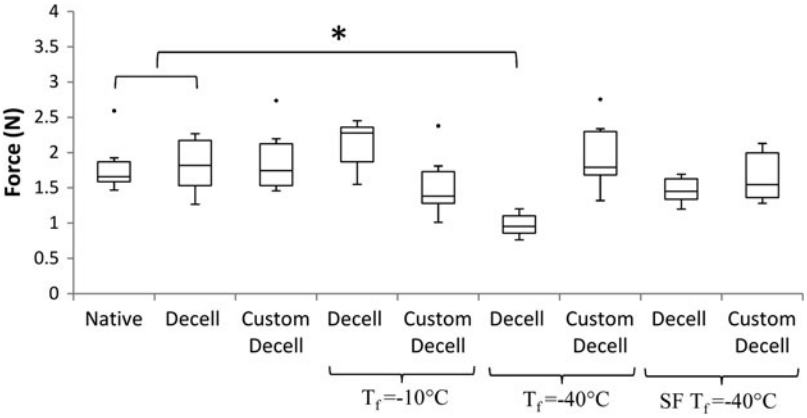

FIG. 7. Suture retention strength for native tissue and decellularized scaffolds. Decellularization, customization, and freeze drying had little effect on the suture retention strength. $T_f = -40°C$ for decellularized scaffolds produced a significant drop in suture retention strength. Statistical significance is indicated as $*p < 0.05$.

for heating to −40°C, small ice crystals are encouraged to recrystallize to produce bigger more contiguous crystals that are more stable and allow for more efficient sublimation.[34] This is effectively an annealing step that guarantees more uniform distribution of stable ice crystals, resulting in even drying and no disruption of the ECM components. The SF $T_f = -40°C$ freeze-drying cycle is the optimum parameters for both the standard decellularized scaffolds used here and our customized scaffolds. This freeze-drying technique is even more effective in the customized scaffolds, as ice crystal distribution is more homogenous to begin with, as the less dense scaffold has more space to promote uniform nucleation. These results further highlight the suitability of our customized scaffold for use in vascular tissue engineering.

Transmural residual stress exists to ensure uniform stress distributions under normal conditions and can change in response to injury or disease.[24,25] The opening angle test relieves the transmural residual stress (Fig. 6B). It has been shown that the individual constituents of the ECM are responsible for the value of θ, with elastin having a residual tension and collagen having a residual compression.[35] Decellularization is known to cause a reduction in opening angle.[23] Our results confirm that not only this effect was observed in the decellularized scaffolds compared with native scaffolds, but also a significant difference was observed between the decellularized and customized scaffolds. Here, we see an excessive compressive component of the scaffold expressing itself as the scaffold sections recoiled to a lesser degree than the intact diameter. Freeze drying further altered the residual stress as a reduction in opening angle was seen across the decellularized freeze-dried scaffolds; this may be due to the collagen fiber disruption in $T_f = -10°C$ and SF $T_f = -40°C$ and the elastin damage in the $T_f = -40°C$. Opening angles for customized scaffolds were significantly increased for each freeze-drying cycle, which reverted the opening angle back toward that of native tissue.

The suture retention tests further verify that the SF $T_f = -40°C$ technique for freeze drying was the most effective. This is a vital test in terms of clinical applicability, as suturing a tissue-engineered construct correctly in place with industry standard sutures is essential for *in vivo* graft performance. This is particularly important, as neo-intimal hyperplasia occurs most often at the anastomosis, and it is at this location that compliance mismatch is most likely.[36] The results from these tests indicate that freeze drying does not significantly alter the suture retention strengths of the decellularized or customized scaffolds, except for decellularized scaffolds in the $T_f = -40°C$ group. Potentially, the elastin disruption due to freeze drying as described earlier has also significantly reduced the suture retention strength, further verifying that this freeze-drying cycle is unsuitable for use with decellularized scaffolds. The SF $T_f = -40°C$ scaffolds were not significantly different, further demonstrating the techniques' applicability for both decellularized and customized scaffolds.

The rationale for this study was to develop a clinically relevant shelf life for decellularized scaffolds. We have initial data which show that scaffolds stored for approximately 6 months appeared fully intact and dried and maintained their integrity on a macro scale. Furthermore, it has been demonstrated for other acellular tissues that freeze-dried storage for 12 months did not affect the mechanical properties of the tissue.[37] In addition, a large number of current commercially available biological scaffolds utilize freeze drying for successful long-term storage.[38] While we do not have data to demonstrate 12 month shelf-life mechanical integrity, the evidence in the literature and our preliminary 6 month data suggests that we will be able to achieve a clinically relevant shelf life. Future work will involve further customization of the freeze-dried decellularized scaffold by the manipulation of injection channels within the media to allow for the rapid introduction of cells and/or therapeutics directly into the dry scaffold before use *in vivo.*

Conclusion

We developed a new freeze-drying protocol for decellularized porcine carotid arteries and customized collagen-digested decellularized porcine carotid arteries. This technique involves snap freezing the scaffolds in liquid nitrogen before insertion into a precooled freeze drier below the T_f at which primary drying occurs. This protocol produces a homogeneous scaffold with undisrupted ECM components and minimal alteration to the overall mechanical properties of the scaffold. This protocol has the potential to be applied to other dense decellularized tissues, and it may have merit in minimizing ECM damage that is induced during the freeze-drying process in other decellularized scaffolds.

Acknowledgments

The authors thank Professor Fergal O'Brien for the use of histology and freeze-drying facilities in the Bone and Tissue

Engineering Research Group, Anatomy Department, Royal College of Surgeons in Ireland.

Disclosure Statement

No competing financial interests exist.

References

1. Weinberg, C., and Bell, E. A blood vessel model constructed from collagen and cultured vascular cells. Science **231,** 397, 1986.
2. Roger, V.L., Go, A.S., and Lloyd-Jones, D.M. Heart Disease and Stroke Statistics—2011 Update: A Report From the American Heart Association. Circulation **123,** e18, 2011.
3. Brar, S., and Stone, G. Advances in percutaneous coronary intervention. Curr Cardiol Rep **11,** 245, 2009.
4. Macchiarini, P., Jungebluth, P., Go, T., Asnaghi, M.A., Rees, L.E., Cogan, T.A., Dodson, A., Martorell, J., Bellini, S., Parnigotto, P.P., Dickinson, S.C., Hollander, A.P., Mantero, S., Conconi, M.T., and Birchall, M.A. Clinical transplantation of a tissue-engineered airway. Lancet **372,** 2023, 2008.
5. Burch, P.T., Kaza, A.K., Lambert, L.M., Holubkov, R., Shaddy, R.E., and Hawkins, J. A. Clinical performance of decellularized cryopreserved valved allografts compared with standard allografts in the right ventricular outflow tract. Ann Thorac Surg **90,** 1301, 2010.
6. Brooks, D.N., Weber, R.V., Chao, J.D., Rinker, B.D., Zoldos, J., Robichaux, M.R., Ruggeri, S.B., Anderson, K.A., Bonatz, E.E., Wisotsky, S.M., Cho, M.S., Wilson, C., Cooper, E.O., Ingari, J.V., Safa, B., Parrett, B.M., and Buncke, G.M. Processed nerve allografts for peripheral nerve reconstruction: a multicenter study of utilization and outcomes in sensory, mixed, and motor nerve reconstructions. Microsurgery **32,** 1, 2012.
7. Gilbert, T.W., Sellaro, T.L., and Badylak, S. F. Decellularization of tissues and organs. Biomaterials **27,** 3675, 2006.
8. Yazdani, S.K., Watts, B., Machingal, M., Jarajapu, Y.P.R., Van Dyke, M.E., and Christ, G.J. Smooth muscle cell seeding of decellularized scaffolds: the importance of bioreactor preconditioning to development of a more native architecture for tissue-engineered blood vessels. Tissue Eng Part A **15,** 827, 2009.
9. Zhao, Y., Zhang, S., Zhou, J., Wang, J., Zhen, M., Liu, Y., Chen, J., and Qi, Z. The development of a tissue-engineered artery using decellularized scaffold and autologous ovine mesenchymal stem cells. Biomaterials **31,** 296, 2010.
10. Tillman, B.W., Yazdani, S.K., Neff, L.P., Corriere, M.A., Christ, G.J., Soker, S., Atala, A., Geary, R.L., and Yoo, J.J. Bioengineered vascular access maintains structural integrity in response to arteriovenous flow and repeated needle puncture. J Vasc Surg **56,** 783, 2012.
11. Borschel, G.H., Huang, Y.-C., Calve, S., Arruda, E.M., Lynch, J.B., Dow, D.E., Kuzon, W.M., Dennis, R.G., and Brown, D.L. Tissue engineering of recellularized small-diameter vascular grafts. Tissue Eng **11,** 778, 2005.
12. Wang, S., Goecke, T., Meixner, C., Haverich, A., Hilfiker, A., and Wolkers, W.F. Freeze-dried heart valve scaffolds. Tissue Eng Part C Methods **18,** 517, 2012.
13. Nakamura, T., Yoshitani, M., Rigby, H., Fullwood, N.J., Ito, W., Inatomi, T., Sotozono, C., Nakamura, T., Shimizu, Y., and Kinoshita, S. Sterilized, freeze-dried amniotic membrane: a useful substrate for ocular surface reconstruction. Invest Ophthalmol Vis Sci **45,** 93, 2004.
14. Nail, S.L., Jiang, S., Chongprasert, S., and Knopp, S.A. Fundamentals of freeze-drying. Pharm Biotechnol **14,** 281, 2002.
15. O'Brien, F.J., Harley, B.A., Yannas, I.V., and Gibson, L.J. The effect of pore size on cell adhesion in collagen-GAG scaffolds. Biomaterials **26,** 433, 2005.
16. Polak, R., and Pitombo, R.N.M. Care during freeze-drying of bovine pericardium tissue to be used as a biomaterial: a comparative study. Cryobiology **63,** 61, 2011.
17. Venkatasubramanian, R., Grassl, E., Barocas, V., Lafontaine, D., and Bischof, J. Effects of freezing and cryopreservation on the mechanical properties of arteries. Ann Biomed Eng **34,** 823, 2006.
18. Müller-Schweinitzer, E. Cryopreservation of vascular tissues. Organogenesis **5,** 97, 2009.
19. Stemper, B.D., Yoganandan, N., Stineman, M.R., Gennarelli, T.A., Baisden, J.L., and Pintar, F.A. Mechanics of fresh, refrigerated, and frozen arterial tissue. J Surg Res **139,** 236, 2007.
20. Sheridan, W.S., Duffy, G.P., and Murphy, B.P. Mechanical characterization of a customized decellularized scaffold for vascular tissue engineering. J Mech Behav Biomed Mater **8,** 58, 2012.
21. Amiel, G.E., Komura, M., Shapira, O., Yoo, J.J., Yazdani, S., Berry, J., Kaushal, S., Bischoff, J., Atala, A., and Soker, S. Engineering of blood vessels from acellular collagen matrices coated with human endothelial cells. Tissue Eng **12,** 2355, 2006.
22. Cho, S.-W., Lim, S.H., Kim, I.-K., Hong, Y.S., Kim, S.-S., Yoo, K.J., Park, H.-Y., Jang, Y., Chang, B.C., Choi, C.Y., Hwang, K.-C., and Kim, B.-S. Small-diameter blood vessels engineered with bone marrow-derived cells. Ann Surg **241,** 506, 2005.
23. Williams, C., Liao, J., Joyce, E.M., Wang, B., Leach, J.B., Sacks, M.S., and Wong, J. Y. Altered structural and mechanical properties in decellularized rabbit carotid arteries. Acta Biomater **5,** 993, 2009.
24. Fung, Y.-C. Biomechanics: Mechanical Properties of Living Tissues. New York: Springer-Verlag, 1993.
25. Humphrey, J. Cardiovascular solid mechanics: cells, tissues, and organs. Appl Mech Rev **55,** B103, 2002.
26. Olausson, M., Patil, P.B., Kuna, V.K., Chougule, P., Hernandez, N., Methe, K., Kullberg-Lindh, C., Borg, H., Ejnell, H., and Sumitran-Holgersson, S. Transplantation of an allogeneic vein bioengineered with autologous stem cells: a proof-of-concept study. Lancet **380,** 230, 2012.
27. McAllister, T.N., Maruszewski, M., Garrido, S.A., Wystrychowski, W., Dusserre, N., Marini, A., Zagalski, K., Fiorillo, A., Avila, H., Manglano, X., Antonelli, J., Kocher, A., Zembala, M., Cierpka, L., de la Fuente, L.M., and L'Heureux, N. Effectiveness of haemodialysis access with an autologous tissue-engineered vascular graft: a multicentre cohort study. Lancet **373,** 1440, 2009.
28. Kakisis, J.D., Liapis, C.D., Breuer, C., and Sumpio, B.E. Artificial blood vessel: The Holy Grail of peripheral vascular surgery. J Vasc Surg **41,** 349, 2005.
29. Atala, A., Bauer, S.B., Soker, S., Yoo, J.J., and Retik, A.B. Tissue-engineered autologous bladders for patients needing cystoplasty. Lancet **367,** 1241, 2006.
30. Cornwell, K.G., Landsman, A., and James, K.S. Extracellular matrix biomaterials for soft tissue repair. Clin Podiatr Med Surg **26,** 507, 2009.
31. Gajiwala, K., and Gajiwala, A.L. Evaluation of lyophilised, gamma-irradiated amnion as a biological dressing. Cell Tissue Bank **5,** 73, 2004.

32. Chang, L., and Pikal, M.J. Mechanisms of protein stabilization in the solid state. J Pharm Sci **98,** 2886, 2009.
33. Hua, Z.-Z., Li, B.-G., Liu, Z.-J., and Sun, D.-W. Freeze-drying of liposomes with cryoprotectants and its effect on retention rate of encapsulated ftorafur and vitamin A. Drying Technol **21,** 1491, 2003.
34. Searles, J.A., Carpenter, J.F., and Randolph, T.W. Annealing to optimize the primary drying rate, reduce freezing-induced drying rate heterogeneity, and determine Tg′ in pharmaceutical lyophilization. J Pharm Sci **90,** 872, 2001.
35. Zeller, P.J., and Skalak, T.C. Contribution of individual structural components in determining the zero-stress state in small arteries. J Vasc Res **35,** 8, 1998.
36. Tiwari, A., Cheng, K.S., Salacinski, H., Hamilton, G., and Seifalian, A.M. Improving the patency of vascular bypass grafts: the role of suture materials and surgical techniques on reducing anastomotic compliance mismatch. Eur J Vasc Endovasc Surg **25,** 287, 2003.
37. Freytes, D.O., Tullius, R.S., and Badylak, S.F. Effect of storage upon material properties of lyophilized porcine extracellular matrix derived from the urinary bladder. J Biomed Mater Res Part B Appl Biomater **78B,** 327, 2006.
38. Badylak, S.F., Freytes, D.O., and Gilbert, T.W. Extracellular matrix as a biological scaffold material: structure and function. Acta Biomater **5,** 1, 2009.

Address correspondence to:
Bruce P. Murphy, PhD
Trinity Centre for Bioengineering
Trinity Biomedical Sciences Institute
Trinity College Dublin
152-160 Pearse Street
Dublin 2
Ireland

E-mail: bruce.murphy@tcd.ie

Received: December 14, 2012
Accepted: April 12, 2013
Online Publication Date: June 25, 2013